Demand Response of a TCL population using Switching-Rate Actuation

Totu, Luminita Cristiana; Wisniewski, Rafal; Leth, John-Josef

Published in:
I E E E Transactions on Control Systems Technology

DOI (link to publication from Publisher):
10.1109/TCST.2016.2614830

Publication date:
2017

Document Version
Early version, also known as pre-print

Citation for published version (APA):
Totu, L. C., Wisniewski, R., & Leth, J-J. (2017). Demand Response of a TCL population using Switching-Rate Actuation. *I E E E Transactions on Control Systems Technology*, *25*(5), 1537 - 1551. https://doi.org/10.1109/TCST.2016.2614830

Demand Response of a TCL population using Switching-Rate Actuation

Luminita Cristiana Totu, Rafael Wisniewski, and John Leth

***Abstract*—This work considers the problem of actively managing the power consumption of a large number of thermostically controlled loads (TCLs), namely a TCL population, and a case-study of household refrigerators. Control is performed using a new randomized actuation that consists of switching units on and off at given rates, while at the same time respecting the nominal constraints on each individual unit. Both the free and the controlled behavior of individual TCLs can be aggregated, making it possible to handle a TCL population as if it were a single system. The aggregation method uses the distribution of the TCLs individual states across the population. The distribution approach has two main advantages. It scales excellently since the computational requirements do not increase with the number of units, and it allows data from individual units to be used anonymously, which solves privacy concerns relevant for consumer adoption.**

I. Introduction

Wind and solar power generation have seen a significant increase in the last decade. This global trend is predicted to continue, and it brings the promise of a more clean and economically stable energy future worldwide. Yet these renewables still represent only a small fraction of the overall power generation [1]. One of the problems is that large scale integration in the power system is challenging. Wind and solar power production have a variable characteristic. While averages over long time scales are predictable, on the shorter time scales the generation output can be volatile and unpredictable. Because the power system needs to be in balance between consumption and production at all times, when a large percentage of the generation has a variable characteristic, the balancing effort increases beyond the possibilities of the traditional grid. Integration levels over 30% require a transformation of the power system [2], [3]. One of the transformations needed is including demand-side as an active participant in the power system operations, both in the planning stage and in the real time balancing services. The idea is to access and organize existing demand flexibility, and utilize it to counteract variability in the grid and, additionally, optimize the economic dispatch of resources [4]–[7].

This work is concerned with a demand response scenario consisting of a large number of thermostat-based appliances, which have an individual on/off operation as a main characteristic. We think of these as many, small and "leaky" thermal storages. These devices are of special interest since they have the potential to deliver a fast, automated response. The focus is on aggregating a very large numbers of units, in order to obtain a total power capacity relevant for power system operations. Using terminology introduced in [8], we want to achieve a control scheme that is *fully responsive* in terms of the aggregated power output and *nondisruptive* to the local unit operation.

The main technical challenges of the control problem are related to the large number of individual units and the distributed structure. Realistic solutions should have a computational complexity that scales well in the number of units, and use communication flows that are feasible under cost and privacy criteria. We will therefore focus on solutions that are aligned with the following three principles. First, actuation should take place via broadcast communication. The network requirements for the actuation channel are thus reduced and communication is fast, since the same signal is sent to all units. Second, the actual physical decisions should take place at the individual unit and account for the local conditions. This guarantees a robust, nondisruptive local operation. Thirdly, measurements on the unit level should be used sparsely and anonymously. This is to ensure that network requirements for the measurement channel are not excessive, and that the overall solution is privacy friendly. Similar implementation principles are discussed also in [9].

The study of large groups of thermostically controlled loads (TCLs), namely TCL populations, started in the 1980s with the works of [10], [11] and [12]. The interest was on modeling oscillations in the power consumption after a planned (direct load control) or unplanned (blackout) interruption. Such oscillations are caused by the synchronization of the thermostatic duty cycles, and can be seen as the free response of a TCL population subject to initial conditions. These early works set in place the "first principles" or "physically based" modeling paradigm for TCL populations. Previous approaches used data-driven models fitted using historical data. The new idea was to first model the main behaviors at the unit level and then model the population behavior as the result of an aggregation operation. The important result in [11] realizes the mathematical aggregation of a homogeneous population of stochastic hybrid systems as a system of partial differential equations (PDEs) with boundary conditions. The PDEs represent the dynamics of the temperature distributions across the "on" and "off" modes in the population, and are obtained in a manner similar to the modeling of physical

All authors are with the Department of Automation and Control, Aalborg University, Denmark e-mail: lct,raf,jjl@es.aau.dk

Manuscript submitted 11th of December, 2014

transport phenomena.

After three decades, the research into TCL populations got a resurgence motivated by the advance of demand response concepts and enabled by the low cost of computing and communication hardware.

For example, the recent modeling work [13] obtains the dynamics of the temperature distributions across the TCL population in another manner, starting with a finite dimensional abstraction. Importantly, the error model is derived for homogeneous populations. Furthermore, approximate error characterizations are also given for heterogeneous populations.

On the control side, different input channel or actuation designs have been proposed to enable demand response. A broadcast actuation method that shifts the set-point temperature of the thermostat is proposed in [14], and subsequently used in other works, e.g., [13], [15], [16]. The broadcast signal consists of a quantity ΔT, which is either positive or negative. All units in the receiving population immediately react by shifting their thermostat band with the ΔT amount. Another broadcast actuation is Toggle Control [17]. This actuation targets subgroups of units from the population based on the location (bin) in the temperature and mode distribution. Individual units switch-on or -off based on a random trial with success probability corresponding to their subgroup. Thus, the broadcast signal consists of a set of switching probabilities, one for each subgroup. A specialized form of Toggle Control, called Switching-Fraction actuation in this work, involves the broadcast of only one or two switching probabilities [18]–[20]. In this case, there are only two target subgroups, the units in mode "on" and the units in mode "off". The broadcast signal consists of a switch-off and a switch-on probability.

The Thermostat Set-Point, Toggle Control and Switching-Fraction all allow for the development of *fully responsive* control algorithms. Furthermore, the Toggle Control and the Switching-Fraction can directly be seen as *nondisruptive*, as the temperature remains bound in the original thermostat band. The Thermostat Set-Point method can also be used in a way that makes it practically *nondisruptive*, e.g. by using only small ΔT band-shift commands. Out of these, we see the Switching-Fraction as having some practical, deployment advantages. Compared to Toggle Control, it does not require local sensors with a high resolution to distinguish between narrow temperature intervals, and the broadcast signal has a smaller footprint. Compared to the Thermostat Set-Point actuation, it has a more direct effect on the power consumption.

Other actuations are present in the literature, but are outside the scope of this work. For example, there are a number of actuations that are meant to be used infrequently and ensure a particular power response, see [21], [22] or [23]. While arguably useful and relevant for different scenarios, we consider these schemes as not fulfilling the *fully responsive* property, as they do not allow a continuous and smooth manipulation of the output power.

This work presents in detail the Switching-Rate actuation, which we briefly introduced in [24], and which extends the Switching-Fraction by desynchronizing the individual TCLs responses in time, across the population. This is important because of the peak power-draw at the TCL compressor start-up. To protect the units against frequent switching, minimum on/off time constraints similar to [25] are considered, and a switch dead-zone is included for temperatures that are too close to the thermostat limit. The Switching-Rate is then used to obtain relevant power responses under two control schemes.

Another contribution of the paper is in the modeling details. In this work, we have followed a modeling approach, for both the free and the actuated dynamics, that starts from a continuous temperature and time domain and then uses numerical tools to obtain discrete approximations. Special care is taken when performing the discretization step to obtain a high quality dynamic matrix, and finite-volume techniques are used to preserve the probability conservation property of the distribution model. Considerations about the positivity property of the discretized dynamics are also made.

The rest of the paper is structured as follows. Section II describes the modeling process. Section III presents model-based control algorithms. Section IV presents a numerical case study and simulation results, showing the demand response capabilities of a TCL population and the effectiveness of the Switching-Rate actuation. Section V concludes the article.

II. Modeling

This work considers cooling units, and in particular domestic refrigerators. As under realistic conditions, the units are independent of each other, do not communicate nor share states. The main object of interest is the aggregated power consumption, which is the sum of the individual power consumptions. The model for an individual TCL is presented first, followed by the aggregation based on distributions[1]. The Switching-Rate actuation is addressed for both the unit and the distribution model.

A. TCL stochastic hybrid model

The model aims to capture only those dynamic characteristics that are relevant at the population level, and is not meant to be high fidelity at the unit level. This approach is prevalent in literature and is supported by verifications using simulation in [18]. The main characteristics to be captured are the thermal dynamics, the hybrid nature of the thermostat operation, and stochasticity. We next present the established unit model, along with considerations about the underlying simplifications.

The basic model is a stochastic hybrid dynamical system (SHS) with two modes corresponding to the "on" or "off"

[1]Distribution in the physical sense, i.e., describing the scattering across a domain.

state of the cooling cycle. When the TCL is "on", it is consuming power and the temperature in the cold compartment is lowering. When the TCL is "off", it is not consuming power and the temperature in the cold compartment is rising due to ambient conditions. The heating and cooling processes are modeled using a lumped approach and first-order dynamics. Although second-order dynamics should be studied for air-conditioning or heat-pump TCLs as argued in [18], this is not considered necessary in the case of domestic refrigerators, since there are no outstanding thermal masses with a pronounced dynamic coupled to cold compartment. Random temperature fluctuations are modeled by a white noise term. Other possible random disturbances, not pursued at this time, are jump processes that would correspond to "door-opening" events. Power consumption is considered to be a positive constant when the mode is "on", and zero when the mode is "off". The assumption is again an idealization, since it is well known (e.g., [26]) that power consumption has a sharp peak at the start of the power cycle (the start of the single phase induction motor) and that it also exhibits an overall first order response pattern (the load dynamics from the vapor-compression cycle), see Fig. 1.

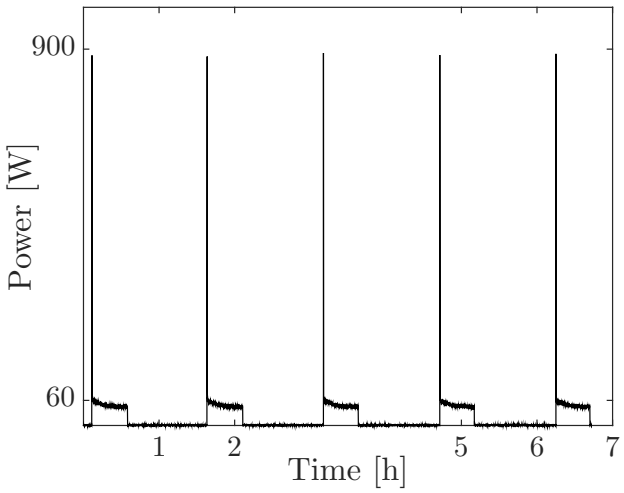

Fig. 1. Power consumption pattern of a real domestic refrigerator (laboratory set-up)

Summing up, the model of a TCL is a SHS of the following form,

$$dT(t) = -\frac{\mathrm{UA}}{C}\left(T(t) - T_a + m(t)\frac{\eta W}{\mathrm{UA}}\right)dt + \sigma dw(t)\ , \tag{1a}$$

$$= \big(\alpha T(t) + \beta + m(t)\gamma\big)dt + \sigma dw(t)\ , \tag{1b}$$

$$z(t) = Wm(t)\ , \tag{2}$$

where $T : \mathbb{R}_+ \to \mathbb{R}$ is the continuously-valued temperature state, $m : \mathbb{R}_+ \to \{0, 1\}$ is the discrete-valued state corresponding to the "off" and "on" modes respectively, $w(t)$ is a white noise process, and $z : \mathbb{R}_+ \to \{0, W\}$ is the power consumption viewed here as model output. The temperature dynamics are expressed using thermal parameters in (1a), and using equivalent first-order system parameters in (1b). All coefficients are considered to be time invariant. In the absence of external control, the dynamics of the discrete-valued state $m(t)$ are given by a standard thermostat mechanism with boundaries at $T_{\min}$ and $T_{\max}$,

$$m(t) = \begin{cases} 1, & T(t) \geq T_{\max}\ , \\ m(t^-), & T(t) \in (T_{\min}, T_{\max})\ , \\ 0, & T(t) \leq T_{\min}\ . \end{cases} \tag{3}$$

Since the discrete-valued state $m(t)$ has discontinuities at the switching times, notation t^- is used to represent limit from left. The convention is that $m(t)$ is right continuous and has left limits.

B. Switching-Rate actuation

The Switching-Rate actuation adds a random component on top of the deterministic thermostat mechanism, see Fig. 2, and is characterized by two transition rates u_0 and u_1. The transition rates are external inputs, to be received over the broadcast channel.

The Switching-Rate random behavior is defined using the Markov chain formalism, see (6). In this way, a TCL that is "off" can be encouraged to consume power using input u_1, while a unit that is "on" can be discouraged from further consuming power using input u_0. At the population level, the magnitude of the input is reflected by the number/percentage of units that actually switch. This externally generated switching is always temperature safe: it can be activated earlier than normal, but not override the thermostat mechanism, which remains in place.

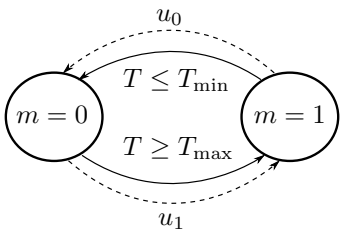

Fig. 2. Dynamics of the discrete state $m(t)$ as a Markov chain, including deterministic, temperature-state dependent transitions (solid line) and random transitions (dashed line).

Additional features are added to prevent the occurrence of multiple switches in a short time interval. Frequent switching can damage the physical components of the TCL such as the compressor, and can invalidate model (1) since the first-order thermal dynamics cannot be expected to be a good approximation on the short time scale. To this end, a timer state $\tau(t) : \mathbb{R}_+ \to \mathbb{R}_+$ with the straightforward dynamic

$$\dot{\tau}(t) = 1 \tag{4}$$

is added to the model, and its value is reset to zero after a switch. Non-thermostatic, external switches are only allowed if a condition of the type $\tau(t) \geq M > 0$ is satisfied. In addition, "safe-zones" are added to ensure that switches do not occur if the temperature is too close to a maximum

or a minimum limit, as they would quickly be reversed by the thermostat action, see Fig 3. Thus, switch-on actions are allowed only if the temperature is in the interval $\mathcal{S}_1$ and switch-off actions are allowed only if the temperature is in the interval $\mathcal{S}_0$,

$$\mathcal{S}_1 = [T_{\min} + \Delta T_1, T_{\max}) \ , \tag{5a}$$

$$\mathcal{S}_0 = (T_{\min}, T_{\max} - \Delta T_2] \ , \tag{5b}$$

where $\Delta T_1, \Delta T_2 < T_{\max} - T_{\min}$.

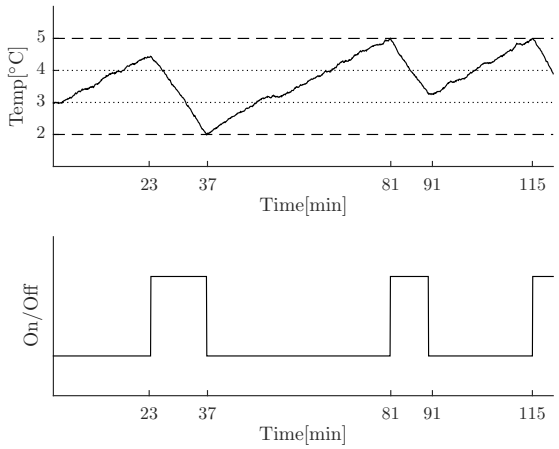

Fig. 3. Temperature and mode trajectory with external actuation. Thermostat actions occur at minutes 37, 81 and 115, and external switches at minutes 23 and 91.

Both the Switching-Fraction (see [18]–[20] for a detailed description) and the new Switching-Rate are randomized actuations, the main difference being the time characteristic. After receiving a broadcast command, the TCL needs to take a decision about "if" and "when" to execute a mode switch. In the Switching-Fraction actuation case, the "when" moment is predefined to be "now", leaving only the "if" question to be answered by the safety checks and a random trial. A consequence of the Switching-Fraction mechanism is that the external switches are tightly synchronized across the population. Since the power consumption of a TCL exhibits a peak after switch-on, see Fig. 1, synchronized switch-on actions lead to synchronized power peaks. The main objective of the Switching-Rate variant is to desynchronize the switch actions across the population. Not only is the switch decision random, but also the time of its occurrence. The mechanism is similar to the jumps in a Poisson process, and as previously indicated, is described by transition rates.

Given a small enough time interval h, and making the informal assumption that the temperature state T does not significantly change its value during this time (does not leave the safe interval $\mathcal{S}_{\bar{i}}$), the probability of a switch event can be written as

$$\begin{aligned} \Pr\big[m(t+h) = \bar{i} \ \big| \ m(t) = i, T(t) \in \mathcal{S}_{\bar{i}}, \tau(t) \geq M \ \big] \\ = u_{\bar{i}} h + o(h) \ , \end{aligned} \tag{6}$$

where $\bar{i} \triangleq 1 - i$, and $u_i \geq 0, \ i \in \{0, 1\}$ are the transition rates. A mathematically rigorous formulation of the above requires the characterization of further stochastic processes elements, such as stopping times and survivor functions. In this work it is only mentioned that the model of a TCL with Switching-Rate actuation can be formally constructed using the notion of general stochastic hybrid systems (GSHSs) [27], [28]. These objects include the three main characteristics of the TCL behavior: dynamics given by stochastic differential equations (SDEs), jumps when the continuous state hits a boundary or according to transition rates, and state resets after jumps.

With a Switching-Rate actuation, switch-on and switch-off events can happen at any point along the continuous time line after the broadcast time, provided that temperature and timer conditions hold safe. In this way, switches are not synchronized across the population, although they might be densely clustered if the received rates u_i have high values.

The Switching-Rate mechanism can be implemented in software on a TCL unit that is equipped with a basic communication and computing digital module, which can be expected from Smart Grid ready appliances. A time-discretized approximation of the GSHS continuous-time behavior, (where temperature state is obtained from measurements, not simulation) can be implemented in different ways. An example is sketched in Alg. 1, where the LOOP function combines the safety checks, numerical inequalities, with a time-discretized version of eq. (6) for the rate-based switch generation. The local sampling time h should be chosen to be relatively small, such that temperature changes can be captured fast by the safety checks, and also such that the rate generation mechanism to be accurate, $u_i \cdot h << 1$.

We recall that in the Switching-Fraction case a single binomial trial with success rate u_i is performed as soon as the broadcast signal is received. This creates synchronization between the units. In the Switching-Rate case, Alg. 1 is performing multiple binomial trials, which are spread out in time and have a scaled-down success rate $u_i \cdot h$. This breaks the synchronization between the units.

Alternatively, an event generation scheme for the Switching-Rate consisting of exponentially generated waiting times together with a mechanism for boundary cross detection could be developed, see also the discussion in [29](Ch.6).

C. Distribution model

The behavior of the TCL can be described, equivalently in effect with the SHS characterization from Section II-A, in terms of the probability density function (pdf) over the hybrid state space $(T, m) \in \mathbb{R} \times \{0, 1\}$,

$$f^i(x,t) = \lim_{dx \searrow 0} \frac{1}{dx} \Pr\big[\ T(t) \in (x, x + dx] \wedge m(t) = i \ \big] \ . \tag{7}$$

The continuous timer state $\tau(t)$ has been omitted for the moment, but will be reintroduced later. Building on elements and results from Markov process theory (e.g., [30], [31]), [11] showed that the dynamic of $f^i(x,t)$ can

Algorithm 1 Switching-Rate

```
global T, m, τ, u_0, u_1
const ΔT_1, ΔT_2, M, h

function BroadcastReceived(new_u_0, new_u_1)
    u_0 ← new_u_0      ▷ "←" denotes an assign operation
    u_1 ← new_u_1
end function

function loop( )          ▷ called 1/h-times per second
    if (m == 1) and (T > T_min) and (T ≤ T_max − ΔT_2) and (τ ≥ M) and (rand() ≤ u_0 · h) then
        m ← 0
    end if
    if (m == 0) and (T < T_max) and (T ≥ T_min + ΔT_1) and (τ ≥ M) and (rand() ≤ u_1 · h) then
        m ← 1
    end if
end function
```

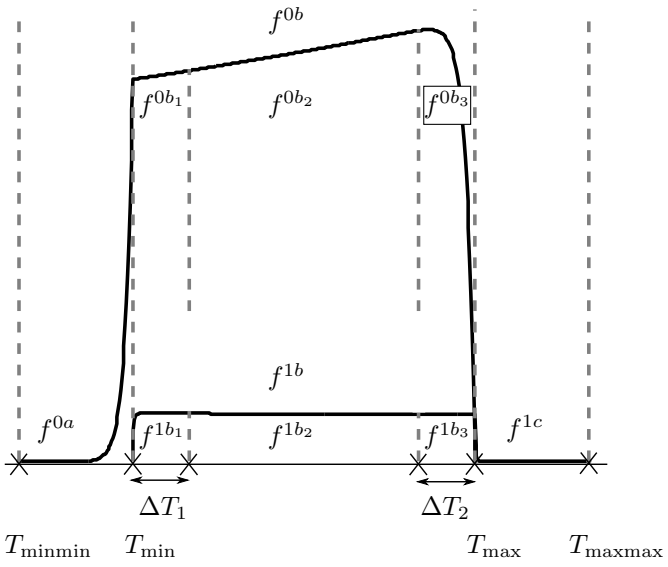

Fig. 4. Partitions of the temperature domain and subcomponents

be described analytically. In particular, the dynamic of $f^i(x,t)$ represents the generator of the forward linear semigroup associated with the SHS model of the TCL. For dynamical systems characterized by regular SDEs, without hybrid elements, this generator is known as the Fokker-Planck equation and can be seen as a transport and conservation law for probability. Therefore, the result in [11] is a type of Fokker-Planck operator specific to the TCL SHS without actuation. The advantage of this modeling is that, unlike the SHS form, a TCL description in terms of the pdf translates almost directly into a (homogeneous) population model. Probability quantities simply change meaning to population fractions, see e.g., [11], [13], [14].

1) Distribution model without actuation: This section introduces the main result from [11] that gives the dynamics of $f^i(x,t)$ in the form of a PDE system with boundary conditions. Before stating the result, some preliminaries are addressed.

The temperature domain is divided into three subsets: the thermostat range $\mathcal{S}_b = [T_{\min}, T_{\max}]$, and $\mathcal{S}_a = (-\infty, T_{\min})$ and $\mathcal{S}_c = (T_{\max}, \infty)$. This is a natural division with respect to the operation of the TCL, and is necessary because boundary conditions apply in the points $T_{\min}$ and $T_{\max}$, and because the pdf $f^i(x,t)$ is not x-differentiable here. Superscript indices will be used to denote subcomponents of the pdf functions $f^i(x,t)$ over the specific partitions, e.g., f^{0a} or f^{1b}. Temperatures outside the thermostat range must be accounted for because of the diffusive component in the thermal dynamics (1). For example, even though the TCL is automatically "on" and starting to cool when $T(t) = T_{\max}$, the temperature might reach values $T(t) > T_{\max}$ due to the contribution of the white noise (diffusive) term. It is also important to note that the pdf corresponding to the off mode, $f^0(x,t)$, is zero-valued on the $\mathcal{S}_c$ domain, because if the temperature becomes greater than $T_{\max}$ the thermostat mechanism ensures that the mode can not remain "off". Similarly, the pdf corresponding to the on-mode, $f^1(x,t)$ is zero-valued on the $\mathcal{S}_a$ domain. In numerical work, the infinity domains limits can be bounded since it is realistic to assume that the temperature inside a working refrigerator will not drop below some T_{minmin} value and cannot rise above some T_{maxmax} value, or equivalently, that probability of this happening is sufficiently low that it can be ignored. These elements are summarized on Fig. 4, using the pdf equilibrium profile corresponding to the refrigerator unit from Section IV. Additionally, Fig. 4 contains notations b_1, b_2 and b_3 for the intervals $(T_{\min}, T_{\min} + \Delta T_1)$, $[T_{\min} + \Delta T_1, T_{\max} - \Delta T_2]$ and $(T_{\max} - \Delta T_2, T_{\max})$, relevant for the actuation part. With this notation, the safe-temperature zones (5) can be expressed as

$$\mathcal{S}_0 = \mathcal{S}_{b_1} \cup \mathcal{S}_{b_2};\ \mathcal{S}_1 = \mathcal{S}_{b_2} \cup \mathcal{S}_{b_3}\ . \tag{8}$$

The evolution of the temperature state $T(t)$ in the interior of the $\mathcal{S}_j$ domains, $j \in \{a, b, c\}$, is driven only by the SDE component (since the discrete dynamics only come into play at the boundaries of the $\mathcal{S}_j$ domains). As a result, the dynamic of the pdf $f^{ij}(x,t)$ on the interior $\mathcal{S}_j$ is given by standard Fokker-Planck equations matching the thermal dynamics (1b) for the corresponding mode,

$$\frac{\partial f^{0j}(x,t)}{\partial t} + \frac{\partial}{\partial x}\Big((\alpha x + \beta) f^{0j}(x,t)\Big) = \frac{\sigma^2}{2}\frac{\partial^2 f^{0j}(x,t)}{\partial x^2}, \quad j \in \{a, b\} \tag{9a}$$

$$\frac{\partial f^{1j}(x,t)}{\partial t} + \frac{\partial}{\partial x}\Big((\alpha x + \beta + \gamma) f^{1j}(x,t)\Big) = \frac{\sigma^2}{2}\frac{\partial^2 f^{1j}(x,t)}{\partial x^2}, \quad j \in \{b, c\}. \tag{9b}$$

The switching dynamics (3) are included in the boundary conditions. We first introduce the probability flows $h^{ij}(x,t)$ as the integral over the temperature (x-) coor-

dinate of the probability fluxes $\frac{\partial f^{ij}}{\partial t}(x,t)$,

$$h^{0j}(x,t) = -(\alpha x + \beta) f^{0j}(x,t) + \frac{\sigma^2}{2}\frac{\partial f^{0j}(x,t)}{\partial x}, \quad (10a)$$

$$h^{1j}(x,t) = -(\alpha x + \beta + \gamma) f^{1j}(x,t) + \frac{\sigma^2}{2}\frac{\partial f^{1j}(x,t)}{\partial x}. \quad (10b)$$

The boundary conditions can then be written as

$$h^{0a}(T_{\text{minmin}},t) = 0,\ h^{1c}(T_{\text{maxmax}},t) = 0, \quad (11a)$$

$$f^{1b}(T_{\min},t) = 0,\ f^{0b}(T_{\max},t) = 0, \quad (11b)$$

$$f^{0b}(T_{\min},t) = f^{0a}(T_{\min},t),$$

$$f^{1b}(T_{\max},t) = f^{1c}(T_{\max},t), \quad (11c)$$

$$h^{0a}(T_{\min},t) = h^{0b}(T_{\min},t) + h^{1b}(T_{\min},t), \quad (11d)$$

$$h^{1c}(T_{\max},t) = h^{0b}(T_{\max},t) + h^{1b}(T_{\max},t). \quad (11e)$$

Equations (11a) represent impenetrable wall conditions, i.e. there is no probability flow out-of or in-to the domain $\mathcal{S}_a$ from the left side, and similarly there is no flow out-of or in-to the domain $\mathcal{S}_c$ from the right side. The rest of the boundary conditions are associated with the thermostat switching mechanism. First, (11b) account for the "absorption" action of the thermostat switch on the diffusion dynamic, causing $\Pr[\ T(t) = T_{\min} \wedge m(i) = 1\ ] = 0$ and $\Pr[\ T(t) = T_{\max} \wedge m(i) = 0\ ] = 0$. Second, the fact that the temperature state does not jump (is not reset) by the switching mechanism is reflected in the continuity condition (11c). Finally, (11d) and (11e) describe of the flow of probability from mode "on" to mode "off" at $T_{\min}$, and the flow of probability from mode "off" to mode "on" at $T_{\max}$.

The above boundary conditions reduce to the more familiar form presented in [11], [14] and others, if they are made explicit by introducing the flow functions expressions (10), and carrying out the arithmetical simplifications. The form presented here, using flow functions h, can also be used in the case when considering other forms for the continuous dynamics of the hybrid branches in (1), e.g. using different diffusion coefficients for each mode.

2) Finite-volume methods: The system (9), together with boundary conditions (11), represents a linear, infinite-dimensional dynamic. We approximate it with a finite-dimensional form using finite-volume methods (FVM) [32], [33]. While other works use a finite-difference approach [15], [34], FVM are arguably more suitable. A main argument is that FVM preserve the invariant of the continuous system in the discretized solution, in this case probability (probability will always amount to 1 in the numerical solution).

FVM consist of three main steps. First, the continuous spatial domain (in this case, the temperature domain) is partitioned using a relatively fine grid of non-overlapping cells[2]. The second step consists of building the FVM equation. This is done by integrating the dynamical PDE equation over a cell of the grid. For a generic conservation dynamic in one spatial dimension x with drift field $\phi(x,t)$, diffusion coefficient $D = \frac{\sigma^2}{2}$, and source term $s(x,t)$,

$$\frac{\partial \rho}{\partial t}(x,t) + \frac{\partial\big(\phi(x,t)\rho(x,t)\big)}{\partial x} = D\frac{\partial^2 \rho(x,t)}{\partial x^2} + s(x,t), \quad (12)$$

integrating over the spatial cell K_q gives

$$\int_{K_q} \frac{\partial \rho}{\partial t}(x,t)dx = \Big(-\phi(x,t)\rho(x,t) + D\frac{\partial \rho(x,t)}{\partial x}\Big)\Big|_{K_q^-}^{K_q^+} + \int_{K_q} s(x,t)dx\ , \quad (13)$$

where $q \in \{1,\dots,N\}$ is the cell index, and K_q^-, K_q^+ are the left and right edge points of the cell. Notice that flow quantities evaluated at K_q^- appear with a negative sign (outgoing) in the dynamic of the cell K_q, and with a positive sign (incoming) in the dynamic of the cell K_{q-1}. The outgoing flow from one cell is incoming flow to the neighbor cell, resulting in the conservative property of the method (in this way, the system invariant will not change/be corrupted by the numerical steps). Next, the left side of (13) can be further expressed as

$$\int_{K_q} \frac{\partial \rho}{\partial t}(x,t)dx = \frac{d}{dt}\int_{K_q} \rho(x,t)dx = \Delta x_q \frac{d\Theta_q}{dt} \quad (14)$$

with Θ_q the average value of $\rho(x,t)$ over the cell K_q and Δx_q the cell size. Equations (13) and (14) can be combined to give the exact expression for the evolution in time of the average quantity Θ_q,

$$\Delta x_q \frac{d\Theta_q}{dt} = \Big(-\phi(x,t)\rho(y,t) + D\frac{\partial \rho(x,t)}{\partial x}\Big)\Big|_{K_q^-}^{K_q^+} + \int_{K_q} s(x,t)dx\ . \quad (15)$$

However, equation (15) is not closed since the right side expression uses the $\rho(x,t)$ terms, which are unknown. The third step thus consists of applying a numerical scheme for approximating the right side of (15) using only $\Theta_q, \Theta_{q+1}, \Theta_{q-1}, \dots$ terms. This step is a combination of reconstruction techniques (interpolation and extrapolation) on stencils, numerical approximation for differentiation and integration operations, and also heuristics such as the up-wind scheme [32]. Once this step is complete, a finite dimensional ordinary differential equation (ODE) system with N equations can be used as an approximation of the original infinite dimensional dynamic.

In the particular case of the TCL PDE system, the temperature sub-domains $j \in \{a,b,c\}$ are each divided into a number N_j of cells, $\mathcal{S}_j = \cup_{q=1}^{N_j} K_{jq}$. It is convenient to use uniform griding, meaning equal cell sizes $\Delta x_{jq} = \Delta x,\ \forall j,q$. As a result of the FVM spatial discretization procedure, the pdf states $f^{ij}(x,t)$ are replaced by vector states $F^{ij} \in \mathbb{R}^{N_j}$, see Fig. 5. These components are ordered as $F = (F^{0a}, F^{0b}, F^{1b}, F^{1c})$, leading to a vector in a state-space of dimension $N^a + 2N^b + N^c = N$.

[2]This is the semi-discrete FVM approach, as only the spatial domain is discretized. The result is a finite-dimensional, continuous-time dynamic in the form of an ordinary differential equation system. The discrete-time dynamics can be obtained later, and separate from the spatial discretization process. Fully-discrete FVM techniques grid the spatial and temporal coordinate simultaneously.

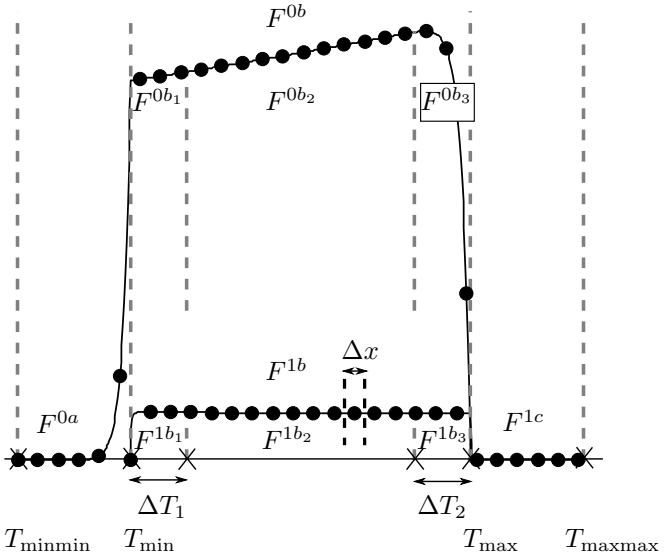

Fig. 5. From the infinite dimensional state f to the final dimensional state $F \in \mathbb{R}^N$, $N = N^a + 2N^b + N^c$, $N^b = N^{b_1} + N^{b_2} + N^{b_3}$.

Subcomponents F^{ib_1}, F^{ib_2} and F^{ib_3} are relevant when considering actuation. Their dimensions are N^{b_1}, N^{b_2}, and N^{b_3}, with $N^{b_1}+N^{b_2}+N^{b_3} = N^b$. Each entry in the vector state F represents the average probability density value in its corresponding cell,

$$F^{ijq}(t) = \frac{1}{\Delta x} \Pr\left[m(t) = i \wedge T(t) \in \mathrm{K}_{jq}\right], \quad i \in \{0,1\},\ j \in \{a,b,c\},\ q \in \{1,2,\dots,N^j\}\ . \tag{16}$$

Because of the linear form of the Fokker-Planck equations and TCL boundary conditions, and by choosing FVM with linear features, the PDE system can be approximated by a linear ODE system,

$$\dot{F}(t) = AF(t)\ . \tag{17}$$

Matrix A is guaranteed to conserve probability i.e., has the property that columns sum to 0.

However, A is not guaranteed to be a proper transition rate matrix, as it can have a number of negative non-diagonal elements. Since the finite dimensional approximation of the PDE system can be seen as a Markov chain representation of the TCL SHS [13], [17], having matrix A in the form of a transition matrix is a desirable property. FVM do not guarantee, in general, the positivity property [35]; however, the FVM scheme proposed in [36] specifically preserves a number of relevant structural properties, among which positivity. This FVM scheme is based on an alternative formulation of the Fokker Planck equation (12)

$$\phi(x,t) \triangleq -\frac{d\mu(x,t)}{dx}\ , \tag{18a}$$

$$\frac{\partial \rho(x,t)}{\partial t} = D\frac{\partial}{\partial x}\left(e^{-\frac{1}{D}\mu(x,t)}\frac{\partial}{\partial x}\left(e^{\frac{1}{D}\mu(x,t)}\rho(x,t)\right)\right) + s(x,t). \tag{18b}$$

The equivalence can be easily checked by expanding the $\frac{\partial}{\partial x}$ differentiation.

The method in [36] is valid also for multidimensional spatial domains. We found numerically that, to obtain a good dynamic approximation, the structure preserving method requires denser grids than more typical schemes, see Sec. IV-A.

3) Distribution model with Switching-Rate: The Switching-Rate actuation can be introduced in the PDE description (9), from where it will propagate into the state-space description (17). We first address the case without the timer locking mechanism. The new terms that are included in the PDE dynamics are marked with under-brackets,

$$\frac{\partial f^{0b}}{\partial t} = -\frac{\partial}{\partial x}\left((\alpha x+\beta)f^{0b}\right) \underbrace{-\lambda_1(x)f^{0b} + \lambda_0(x)f^{1b}}_{} + \frac{\sigma^2}{2}\frac{\partial^2 f^{0b}}{\partial x^2}\ , \tag{19a}$$

$$\frac{\partial f^{1b}}{\partial t} = -\frac{\partial}{\partial x}\left((\alpha x+\beta+\gamma)f^{1b}\right) + \underbrace{\lambda_1(x)f^{0b} - \lambda_0(x)f^{1b}}_{} + \frac{\sigma^2}{2}\frac{\partial^2 f^{1b}}{\partial x^2}\ , \tag{19b}$$

where

$$\lambda_1(x) = \begin{cases} u_1,\ x \in \mathcal{S}_1, \\ 0,\ x \notin \mathcal{S}_1, \end{cases} \quad \lambda_0(x) = \begin{cases} u_0,\ x \in \mathcal{S}_0, \\ 0,\ x \notin \mathcal{S}_0. \end{cases} \tag{19c}$$

The terms $u_1 f^{0b}$ and $u_0 f^{1b}$ give a fitting dynamic for the exchange of probability from off-to-on and on-to-off respectively due to the design of the external switching, see the infinitesimal contribution given in (6).

The discontinuity in the $\lambda_i(x)$ functions, and thus the discontinuity in the PDE coefficients, may raise concerns. The effect of the discontinuity in the coefficients, combined with the smoothing effect of the diffusion term, is that the solution remains continuous but is non-differentiable at points $T_{\text{min}} + \Delta T_1$ and $T_{\text{max}} - \Delta T_1$, similar to the behavior at T_{min} and T_{max}. The rigorous formulation is then to split the solutions f^{ib} into subcomponents b_1, b_2 and b_3, and connect these with boundary conditions using flow functions h, that is

$$f^{ib_1}(T_{\text{min}} + \Delta T_1, t) = f^{ib_2}(T_{\text{min}} + \Delta T_1, t),$$
$$f^{ib_2}(T_{\text{max}} - \Delta T_2, t) = f^{ib_3}(T_{\text{max}} - \Delta T_2, t), \tag{20a}$$
$$h^{ib_1}(T_{\text{min}} + \Delta T_1, t) = h^{ib_2}(T_{\text{min}} + \Delta T_1, t),$$
$$h^{ib_2}(T_{\text{max}} - \Delta T_2, t) = h^{ib_3}(T_{\text{max}} - \Delta T_2, t). \tag{20b}$$

FVM can again be applied to reduce the PDE dynamics to a finite dimensional form. The resulting system has the following form,

$$\dot{F}(t) = AF(t) + u_0(t)B_0F(t) + u_1(t)B_1F(t). \tag{21}$$

We remark that the Switching-Rate input enters the dynamic equations in a bilinear form in (21) (and later (28)), which is also the case for the Switching-Fraction, and for the Thermostat Set-Point actuation [15].

We highlight also the main difference between the Switching-Rate and the Switching-Fraction, namely the continuous-time nature of the first, and the discrete-time

nature of the second. For piecewise-constant input signals, discrete-time form of (21), is

$$F(k+1) = e^{\left(A+u_0(k)B_0+u_1(k)B_1\right)\Delta t}F(k), \tag{22}$$

which is not equivalent to the Switching-Fraction model,

$$F(k+1) = \left(e^{A\Delta t} + u_0(k)B_0 + u_1(k)B_1\right)F(k)\ . \tag{23}$$

4) Timer-Lock modeling: The modeling principle for the timer-lock is to explicitly track the part of the pdf that becomes locked for the external actuation. Two density functions are introduced to correspond to the locked condition for mode "off" and for mode "on", $L^0 : (T_{\text{minmin}}, T_{\max}) \times [0, M) \times [0, \infty) \to \mathbb{R}_+$ and $L^1 : (T_{\min}, T_{\text{maxmax}}) \times [0, M) \times [0, \infty) \to \mathbb{R}_+$,

$$L^i(x, y, t) = \lim_{\substack{dx\searrow 0\\ dy\searrow 0}} \frac{1}{dxdy}\ \Pr\ \big[\ T(t) \in (x, x+dx] \wedge \\ \wedge\, \tau(t) \in (y, y+dy]\ \wedge m(t) = i\ \big]\ . \tag{24}$$

The part of $f^i(x,t)$ which remains responsive to the actuation is evaluated by subtracting the probability of being locked, and the following updates are made to (19a) and (19b),

$$\lambda_1(x)f^{0b} \to \lambda_1(x)\left(f^{0b} - \overbrace{\int_0^M L^0(x,y,t)dy}^{\text{amount of locked } f^{0b}}\right)\ , \tag{25a}$$

$$\lambda_0(x)f^{1b} \to \lambda_0(x)\left(f^{1b} - \overbrace{\int_0^M L^1(x,y,t)dy}^{\text{amount of locked } f^{1b}}\right)\ . \tag{25b}$$

The dynamics of L^i are given by standard Fokker-Planck equations in the two-dimensional state space (T, τ) (temperature and timer state), with the underlying process driven by (1b) and (4), with no external switching contributions. The dynamics are thus,

$$\frac{\partial L^i}{\partial t}(x,y,t) = -\frac{\partial}{\partial x}\Big((\alpha x + \beta + i\gamma)L^i(x,y,t)\Big) - \\ - \frac{\partial}{\partial y}L^i(x,y,t) + \frac{\sigma^2}{2}\frac{\partial^2}{\partial x^2}L^i(x,y,t)\ , \tag{26}$$

with boundary conditions,

$$h^{L0}(T_{\text{minmin}}, y, t) = 0,\ h^{L1}(T_{\text{maxmax}}, y, t) = 0, \tag{27a}$$

$$L^1(T_{\min}, y, t) = 0,\ L^0(T_{\max}, y, t) = 0, \tag{27b}$$

$$L^i(x, 0, t) = \lambda_{\bar{i}}(x,t)\big(f^{\bar{i}b}(x,t) - \int_0^M L^{\bar{i}}(x,y,t)dy\big). \tag{27c}$$

Equations (27a) represent impenetrable walls conditions where the probability flow h defined in (10) is zero, and (27b) represent absorbing boundaries due to the thermostat action. Finally, (27c) accounts for the incoming probability of a new switching event and the zero reset of the timer state. This is a condition that has discontinuities in the x-space and in time, see (19c) and the fact that $u_i(t)$ is, due to the nature of broadcast communication, a piecewise constant function. Again, discontinuities can be a problem for the current mathematical description. A solution can be to modify the TCL behavior to an ideal version where a smooth approximate of the $\lambda_i(x,t)$ is used. However, such modifications do not change any of the practical considerations and have little impact on the results of the computational algorithms, including the FVM procedure. The main difference introduced by the modeling of the locking mechanism is that a two dimensional FVM scheme needs to be used for the state L^i. The final form of the finite-dimensional dynamic is,

$$\dot{X}(t) = A^X X(t) + u_0(t)B_0^X X(t) + u_1(t)B_1^X X(t)\ , \\ X = (F,\ L^0,\ L^1)\ , \tag{28}$$

where $L^0 \in \mathbb{R}^{(N_a+N_b)M_d}$, $L^1 \in \mathbb{R}^{(N_b+N_c)M_d}$, $X \in \mathbb{R}^{N(M_d+1)}$, and M_d is the number of grid cells with size Δy used to discretize the timer-state domain $[0, M]$. A linear coordinate change can be used to create a Markov chain formulation, by separating the unlocked from the locked states,

$$X' = \Big(\ F^0 - \Delta y \sum_{l=1}^{M_d} \overbrace{L^0_{(l-1)N_{a+b}+1:lN_{a+b}}}^{\text{off, locked, } \tau\in[(l-1)\Delta y, l\Delta y)}\ , \\ F^1 - \Delta y \sum_{l=1}^{M_d} \overbrace{L^1_{(l-1)N_{b+c}+1:lN_{b+c}}}^{\text{on, locked, } \tau\in[(l-1)\Delta y, l\Delta y)}\ , \\ L^0,\ L^1\ \Big) = T_X X\ , \tag{29}$$

where T_X denote the coordinate change defined by the left-hand side of (29) and X' denote X in the new coordinates.

Locking effects after a thermostatic switch are not considered. The reason why this is not necessary is due to the temperature safe-zones feature. After a thermostatic switch, the unit is prevented from switching again until it is some distance ΔT away from the thermostat boundary. This temperature distance can be chosen such that its effects are practically equivalent to a timer condition.

This completes the main part of the Switching-Rate modeling.

5) Model output and extension: The expected power consumption output of a TCL can be obtained by calculating the total probability of a unit being "on", and scaling it with the power rating parameter W,

$$z(t) = CF(t), \tag{30}$$

with $C = W\Delta x\begin{bmatrix}0_{1\times(N_a+N_b)} & 1_{1\times(N_b+N_c)}\end{bmatrix}$.

The Fokker-Planck approach to modeling the distribution dynamics can also be used when considering other elements in the TCL model, such as nonlinear terms or jump noises. Another remark is that coefficients and parameters characterizing the dynamical behaviors can take different values in mode "on" compared to mode "off", for example the entire drift field, the diffusion coefficients, and temperature safe zones ΔT, and the timer setting M.

6) Population Heterogeneity: As mentioned, when considering a large group of units with identical parameters (a homogeneous population), probabilities simply change meaning to fractions. This means that models (21) and (28) can be initialized in with values for F (or X) reflecting the fraction distribution of the temperature and mode (and timer) values across the population, instead of the probability distribution of a unit's initial state. The dynamics with naturally propagate the distributions over time and under inputs.

Small heterogeneities of the TCL population should not cause severe modeling errors, but large heterogeneities will cause a significant departure from the homogeneous case. However, exact modeling of heterogeneous population is impractical since it suffers from "curse of dimensionality" (the distribution state-space needs to be extended with an extra dimension for each parameter). Therefore, heterogeneity is not explicitly accounted for in the distribution model. Instead, this work makes use of the fact that the switching actuation has a certain amount of robustness to model variations due to its percentage formulation, and furthermore, measurements and estimations can be used to periodically update the distribution state in real-time operation.

For a more pronounced dispersion of parameters, a clustering strategy e.g., [18], should be applied first. Therefore, the models and control proposed in this work are to be applied for each individual cluster in a heterogeneous population. In the numerical simulations, moderate levels of heterogeneity are considered for the TCL population.

III. Model-based Control Algorithms

This section presents two model-based control algorithms that can be used to manipulate the aggregated power consumption of the TCL population via the Switching-Rate actuation. The control objective is to have the power output track an input reference. At the end, considerations are made about the measurement channels.

A. Control System

The TCL population model has a continuous-time, bilinear [37], [38], homogeneous input form, for both the basic and timer-lock augmented versions,

$$\dot{F}(t) = \big(A + \sum_i u_i(t) B_i\big) F(t), \tag{31a}$$

$$\dot{X}(t) = \big(A^X + \sum_i u_i(t) B_i^X\big) X(t)\ , \tag{31b}$$

with $u_i \in [0, u_{\max}]$. The aggregated power consumption is a linear combination of the states,

$$z_a(t) = nCF(t), \tag{32}$$

where n is the number of units in the population, and for the timer-lock augmented system F is recovered as the first N-coordinates in X according to (28).

The free dynamics of the system are given by matrix A, which has stable eigen values, except one which is exactly zero. This is due to the FVM procedure producing a dynamic matrix that conserves the probability invariant of the system state, by having columns that sum to 0. This fact can be used to reduce the system dimension by one state. Given an initial state $F(0)$ such that the sum of its elements is f (in particular $f = \frac{1}{\Delta x}$), the sum of the $F(t)$ elements will remain equal to f. Therefore, one of the states can be written as the difference between f and the sum of all others.

$$F(t) = \begin{bmatrix} \bar{F}(t) \\ F_N(t) \end{bmatrix},\ \bar{F} \in \mathbb{R}^{N-1}, F_N \in \mathbb{R}, \tag{33a}$$

$$\begin{bmatrix} \dot{\bar{F}} \\ \dot{F}_N \end{bmatrix} = \left(\begin{bmatrix} A_{11} & A_{12} \\ A_{21} & a_{22} \end{bmatrix} + \sum_i u_i \begin{bmatrix} B_{i,11} & B_{i,12} \\ B_{i,21} & b_{i,22} \end{bmatrix} \right) \begin{bmatrix} \bar{F} \\ F_N \end{bmatrix}, \tag{33b}$$

$$F_N = f - 1_{N-1}^T \bar{F}, \tag{33c}$$

$$\begin{aligned} \dot{\bar{F}} &= A_{11}\bar{F} + A_{12}(f - 1_{N-1}^T \bar{F}) + \sum_i u_i B_{i,11} \bar{F}, \\ &= \left(\bar{A} + \sum_i u_i \bar{B}_i \right) \bar{F} + \bar{a}. \end{aligned} \tag{33d}$$

In (33b) matrix $B_{i,12} = 0$ for the switching actuation (because F_N belongs to the c-temperature domain, which is not affected by the actuation), in (33d) $\bar{A} = A_{11} - A_{12}1_{N-1}^T \in \mathbb{R}^{(N-1)\times(N-1)}$, $\bar{a} = A_{12} f$ and $\bar{B}_i = B_{i,11}$. The dynamical system matrix $\bar{A}$ of the transformed system is Hurwitz. Furthermore, a change of variables can move the equilibrium state of the affine system (33d) to 0, resulting in linear, stable free dynamic at the expense of an added affine input term,

$$\bar{F}_0 = \bar{F} + \bar{A}^{-1}\bar{a}\ , \tag{34a}$$

$$\dot{\bar{F}}_0 = \left(\bar{A} + \sum_i u_i \bar{B}_i \right) \bar{F}_0 - \sum_i u_i \overbrace{\bar{B}_i \bar{A}^{-1} \bar{a}}^{\bar{b}_i}\ . \tag{34b}$$

In summary, we started with matrix A which has a one-dimensional null-space, identified the equilibrium state in the null-space by the "sums to f" constraint given by the initial state, and then shifted the equilibrium to zero using a change of variable. Notice also that the equilibrium distribution can be calculated as

$$\bar{F}_e = \big[-\bar{A}^{-1}\bar{a}, \qquad f + 1_{N-1}^T \big(\bar{A}^{-1}\bar{a} \big) \big]\ . \tag{35}$$

The same process of changing from a marginally stable to a fully stable dynamic description can be applied to the A^X timer-lock system matrix. Since the algorithms used in this work do not require strict stability, in the following we will continue to use the forms (31).

B. Input Reference Tracking

This section presents two control algorithms for tracking an external power reference. By necessity (the geographically distributed nature of the control structure), all control algorithms operate in discrete-time. Thus, the TCLs maintain the switching rates u constant until the next broadcast event (piecewise constant actuation). The

first algorithm uses switch-off and switch-on actions one at a time, while the second algorithm uses an energy storage heuristic and simultaneous switch-off and switch-on actions. The algorithms use the distribution model as internal model, and measurements of the total power consumption at every step, perform calculations or optimizations over short time horizons, and require an estimate for the initial state (which is expected to be close to equilibrium in the absence of actuation). The algorithms can benefit from - but *do not* require - frequently updated state information. The control structure is shown in Fig. 6.

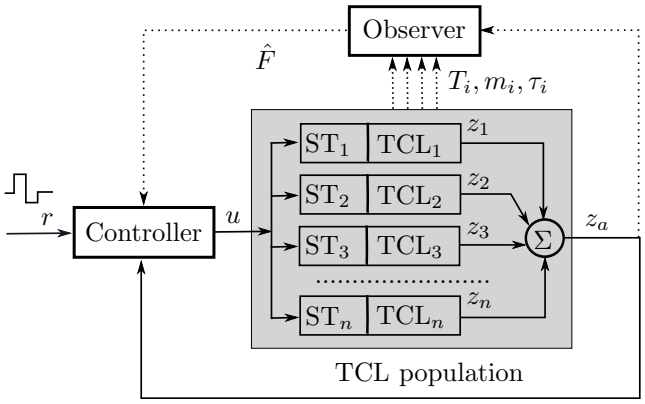

Fig. 6. Controller structure. The dotted lines indicate signals with low update frequency.

1) Basic reference tracking: The main elements of the first control strategy are sketched in Alg. 2. This is a predictive scheme with a single time-step lookahead. First, a prediction is made about the power output in the absence of control. If this is bigger than the reference r, the switch-off action is selected for activation. In the opposite case, the switch-on action is selected. Consequently, the main step consists of calculating the precise input value that would bring the internal model of the controller to the desired reference. An input-output linearization technique [39] is used, together with the simplified assumption that the output velocity remains constant in the control sample time Δt,

$$z_a(k+1) = z_a(k) + \dot{z}_a(k)\Delta t \ , \tag{36a}$$

$$\dot{z}_a(k) = nCAF(k) + u_i(k)nCB_iF(k) \ , \tag{36b}$$

$$u_i(k) = \frac{-nCAF(k) + v}{nCB_iF(k)} \ , \tag{36c}$$

$$z_a(k+1) = z_a(k) + v\Delta t \ , \tag{36d}$$

$$v = \frac{r(k+1) - z_a(k)}{\Delta t} \ , \tag{36e}$$

where (36d) is obtained from (36a)-(36c). For robustness to heterogeneity and other prediction errors, the actuation is wrapped in an error integration structure (PI control), preferably with anti-windup. Algorithm 2 is suitable for both the simple and the augmented models, since the computation load is light. In Alg. 2, the integration gain K_i is a design parameter.

While arguably practical, Alg. 2 manages the power flexibility of the TCL population in a simplistic manner.

Algorithm 2 Step k

$e = K_i e + z_a(k) - r(k)$ ▷ tracking error at k
$e_p = nCe^{A\Delta t}F(k) - (r(k+1) - e)$
▷ predicted error at $k+1$ if no actuation is used
if $e_p > 0$ **then** ▷ Need to decrease output, use u_0
$u_0(k) = \textsc{Control}(B_0)$
else if $e_p < 0$ **then** ▷ Need to increase output, use u_1
$u_1(k) = \textsc{Control}(B_1)$
end if

---

function CONTROL(B)
$v = \big(r(k+1) - z_a(k)\big)/\Delta t$
$u = \big(-nCAF(k) + v\big)/\big(nCBF(k)\big)$
$u = \textsc{Limit}(u,0,u_{\max})$ ▷ saturation cut
$F(k+1) = e^{(A+uB)\Delta t}F(k)$
return u
end function

This is because, in most cases, there exists more than one actuation option for bringing the output of the system to the reference power consumption $r(k+1)$. By having a lookahead horizon of just one step, and using a preset strategy for choosing between the actuation options, Alg. 2 is not able to track challenging references. An example of a challenging reference is a step-down to zero.

2) Zero power reference: The second control algorithm is an example of heuristics that can maintain a zero power-reference over a time horizon of reasonable length. This control uses a slightly modified version of the switching action. Since the TCL temperature sensor is already required to distinguish between three domains in the thermostat band (b_1,b_2,b_3), we can consider an actuation variant with four input channels: u_{0b_1}, u_{0b_2}, u_{1b_2} and u_{1b_3}. This means that it is possible to use one switch-off rate for the on-units in the temperature range $\mathcal{S}_{b_1}$ and another for the on-units in the temperature range $\mathcal{S}_{b_2}$, and similarly, two different switch-on rates for the off-units in the $\mathcal{S}_{b_2}$ and $\mathcal{S}_{b_3}$ ranges.

The control strategy is composed of three phases, sketched in Fig. 7. Each phase of the strategy is controlled by a different algorithm. In the first phase, the units are pushed away from the right (hot) thermostat band using the switch-on action u_{1b3}. In order to keep the power consumption close to a normal level, this action must be compensated by switching-off units from the left (cold) side of the thermostat using the u_{0b1}. The combined effect is equivalent to a narrowing of the thermostat band to the $\mathcal{S}_{b_2}$ interval. In this operation mode, the duty cycle of a unit will be only slightly higher than the normal value, and the aggregated power output of the population can remain close to the baseline value. The second phase corresponds to the zero power consumption period. The on- and off-distributions are now collected in the midband range $\mathcal{S}_{b_2}$. Therefore, it is possible to switch-off all units using input u_{0b_2}. Power consumption will remain zero as the collected off-distribution is slowly moving right (heating) across the $\mathcal{S}_{b_1}$ domain and up until the $T_{\max}$ threshold of the

thermostat is reached. The third stage is recovery. The population needs to be controlled so as to slowly return to the equilibrium distribution, while maintaining a power consumption level close to the baseline. We do not solve the recovery problem in this work, but simply apply Alg. 2 to return power consumption to the baseline level. We notice that in this way the system output is returned and maintained to the equilibrium values, but not also the system state.

Algorithm 3 details this second control strategy. The storage phase consists of a multi-objective optimization over each control sample time,

$$\underset{u_{1b_3}(k),u_{0b_1}(k)}{\text{minimize}} \; [\; -u_{1b_3},\; \sum_{p=1}^{P} \left(nCX(p) - r(p)\right)^2 \;]$$

subject to

$$X(0) = F(k)\ ,$$
$$X(p+1) = \exp\big(\big(A + \sum_{j\in\{1b_3,0b_1\}} u_j(k)B_jX(p)\big)\tfrac{\Delta t}{P}\big)X(p)\ ,$$
$$u_{1b_3}(k) \geq 0\ ,$$
$$u_{0b_1}(k) \geq 0\ .$$

We want to switch-on as many units as possible using u_{1b3}, and compensate by the switching-off action u_{0b1} in order to keep the power consumption close to a baseline reference. To avoid large fluctuations within the control sample time Δt, the reference tracking objective is formulated using a series of p intra-period time points. The multi-objective optimization was implemented using `fgoalattain()` MATLAB® function, based on the goal attainment method [40]. While the optimization approach has the potential of becoming computationally heavy, it is sufficient to use the unaugmented distribution model for both populations with and without minimum on/off time constraints. This is because the input actions are well separated between different temperature zones, thus also separated in time, and the locking effect is inherently respected. With this observation, Alg. 3 remains computationally feasible.

Algorithm 3 Step k

if phase(k+1) == "Storage" **then**
  $e = K_i e + z_a(k) - r(k)$ ▷ tracking error at k
  $[\ u_{0b_1}(k),\ u_{1b3}(k)] = \textsc{Optim}(r(k+1) - e)$
else if phase(k+1) == "Discharge" **then**
  $u_{0b_1}(k) = u_{\max},\ u_{0b_2}(k) = u_{\max}$
else if phase(k+1) == "Recovery" **then**
  use Algorithm 2 ▷ Partial recovery
end if

---

function Optim(r)
  $p = 5$ ▷ no. of intra-period points
  ir = linspace($z_a(k)$,r,$p+1$)
    ▷ intra-period reference profile
  lb = [0,0], ub =[$u_{\max}$, $u_{\max}$] ▷ lower/upper bounds
  u = min-multi-objective(@objectives, lb, ub)
  return u
end function
function objectives(u)
  $A_{dn} = e^{(A+u(1)B_{0b1}+u(2)B_{1b3})(\Delta t/p)}$
  $F_p = F(k),\ \text{obj}(1) = 0$
  for $j = 1$ to p **do**
    $F_p = A_{dn}F_p$
    $\text{obj}(1) = \text{obj}(1) + \big(CF_p - \text{ir}(j)\big)^2$
  end for
  $\text{obj}(2) = -u(2)$ ▷ or equiv. $-u(1)$
  return obj
end function

C. Measurements

The main measurement used by the control algorithm is the total power consumption signal. This is the driving signal of the control loop structure. In this work, the TCL population has been considered in isolation, but in a realistic scenario aggregate power measurements from the electrical grid will include other consumption. Therefore, a method would be needed to separate the contribution of the TCLs from the total consumption data. However, the control objective is not the TCL consumption per se, but rather the total consumption in an area (or portfolio). As long as the control objective can be measured, it can be used directly (without separation) to create the control error signal.

Monitoring the distribution state of a TCL population over time requires individual unit measurements. The advantage of the distribution approach is that individual state measurements can be infrequent, partial and are used anonymously. Individual unit measurements consists of the temperature and mode (and timer) data from a limited number of units in the population, e.g., 10% or 20%. These can be processed to create a distribution measurement $\tilde{F}$. The error of such a distribution measurement can be characterized using the variance and covariance properties of the multivariate hypergeometric distribution. This is because by extracting a finite number of units n_m from

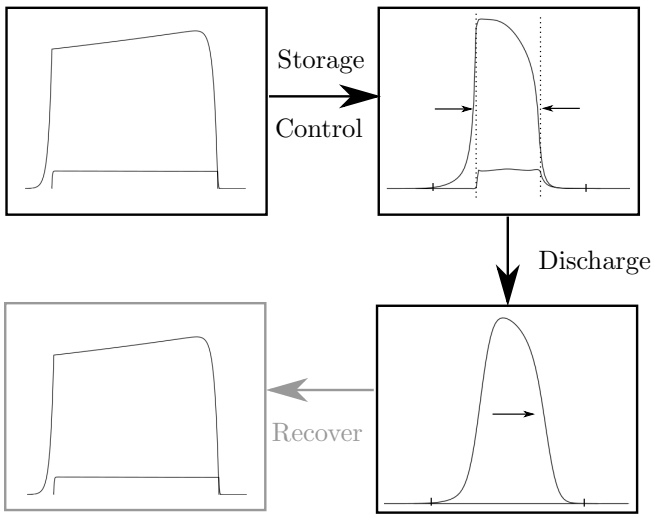

Fig. 7. The stages of the second control algorithm.

the TCL population with $n > n_m$ units and N possible outcomes, we are effectively performing a "draws without replacement" random experiment. Furthermore, the dynamical models (31), could be equipped with error models, see the approach in [13]. We do not, however, address the complete estimation problem in this work.

IV. Numerical simulations

This section contains numerical results on a case-study for domestic refrigerators. The equivalent thermal parameters used for the TCL model (1a) are listed in Table I. The actuation parameters are the minimum on/off time $M = 300s$, the temperature safe-zones are $\Delta T_1 = \Delta T_2 = 1°C$, and $u_{\max} = 2$.

TABLE I
Parameters of the TCL

C (J/K)	UA (W/K)	T_a ($°C$)	W (W)
93920	1.432	24	100
η	σ ($°C/s$)	$T_{\min}(°C)$	$T_{\max}(°C)$
2.8	0.0065	2	5

In all cases, a population of 10000 units is considered. In addition to the homogeneous population, two types of heterogeneities, each with three increasing levels, have been tested. The parameters have been randomly distributed around the mean values from Table I according to a 3σ-truncated Gaussian distribution with standard deviations of 5%, 10%, and 15%, and according to a uniform distribution with standard deviations of 10%, 20%, and 30%. The C, UA, T_a, η, W, and σ parameters have been affected, while the thermostat range, temperature safe-zones and the minimum on/off time are the same across the population. The TCL population has been simulated using Monte Carlo techniques. Each of the 10000 SHS models is run individually with a sample rate of $0.1s$. For control, a broadcast rate $\Delta t = 60s$ has been used.

A. FVM results

We first give a qualitative and quantitative comparison for the dynamical system matrix A obtained with different FVM implementation. In all cases, the FVM grid is uniform, with domain boundaries $T_{\text{minmin}} = 1.5°C$ and $T_{\text{maxmax}} = 5.5°C$. Four cases are compared: a second order up-wind scheme with a coarse (a) and dense (b) grid, and the structure preserving FVM (see end of Sec. II-C2) on a coarse (c) and on a dense (d) grid.

TABLE II
Dynamic matrix A

	Δx	N	Positivity	Duty Cycle
(a)	0.0385	182	No	0.105
(b)	0.01	700	No	0.105
(c)	0.0385	182	Yes	0.04878
(d)	0.0025	2800	Yes	0.1046

The duty cycle calculation is done using the equilibrium distribution computed by (35) and evaluating the percentage of represented by the total area under the on-distribution. It is used as an indicator for the absolute error of the FVM schemes. The duty cycle for a TCL with parameters from Table I is close to 0.105 value. Fig. 8 shows the equilibrium distributions obtained from the four methods. It can be seen that the second order up-wind scheme (a) is not positive, and shows the spurious oscillation effects (see Godunov's order barrier theorem, [33] ch.13), but both these effects are reduced when the grid size is reduced in scheme (b). The structure preserving schemes (c) and (d) are positive, but slower to converge, and as a result the distribution (and duty cycle) of coarse scheme (c) has significant errors. Although accuracy criteria would suggest using schemes (d) or (b), scheme (a) has the advantage of a small computational footprint, and proves to capture the dynamical behavior suitably well for control algorithms.

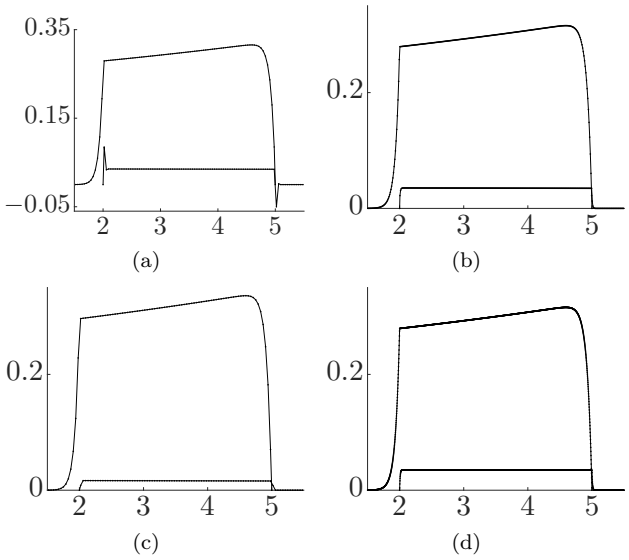

Fig. 8. Equilibrium distributions as obtained using the second order up-wind coarse and dense schemes (a) and (b) respectively, and the structure preserving coarse and dense schemes (c) and (d) respectively. The grid parameters are given in Table II.

Augmented systems have a higher dimensionality. The spatial discretization and overall matrix size used in the following control simulations is given in Table III.

TABLE III
Augmented dynamic matrix A^X

	Δx	Δy	N
A^X	0.0385	30s	2002

B. Free response simulations

Figure 9 shows the free response from an initial state where all units are initially off and have the same temperature, its value close to the hot threshold of the thermostat.

This synchronized initial state showcases the oscillatory nature of the power response, and the differences between the homogeneous and heterogeneous populations. A main

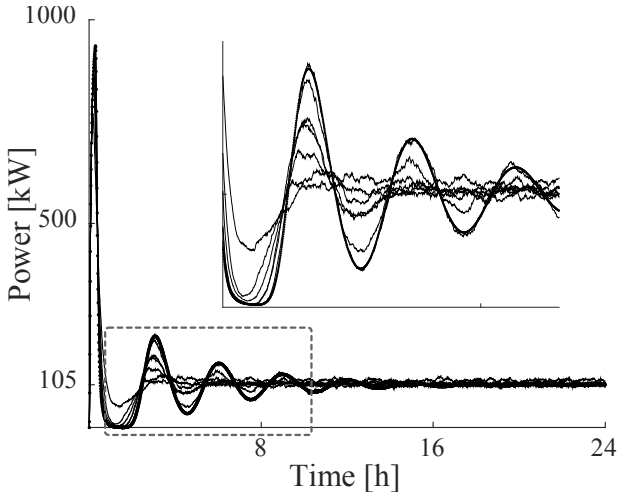

Fig. 9. Free response of TCL populations from a synchronized initial state. The thick line is the distribution model response, while the thin lines are the responses of TCL populations with different levels of heterogeneity.

and well-known characteristic of heterogeneous populations is that they desynchronize and reach the equilibrium state faster. On the other hand, the model error is small for the homogeneous population, and increases with heterogeneity.

C. Control simulations

The TCL populations are known to initially be close to equilibrium. No individual measurements are used for the duration of the 2 hours control horizon, meaning that the model is run in open loop to generate the state estimations required by the algorithms. The measurements of the aggregate power consumption are assumed to be perfect (the simulation does not add error terms to this signal), see the discussion in Section III-C.

Algorithm 2 is tested using two piecewise constant references. Reference I is a repeated sequence consisting of a moderate step-up doubling the baseline, followed by a step-down to zero, placed in between baseline values. Results are shown in Fig. 10. The control is able to follow the step-up section, as this reference lies comfortably within the power consumption flexibility, but cannot reach the zero-level of the step-down section.

Reference II consists of a single step-down to zero. Results are shown in Fig. 11. Once again, the control is not able to reach zero power consumption. The only way to guarantee a zero consumption is to move units away from both the "off" and "on" b_3 zones. This strategy is showcased by Alg. 3. Nevertheless, Alg. 2 is arguably a practical, efficient and *fully responsive* control scheme.

Algorithm 3 performs the storage control and then enters the discharge phase, see Fig. 7. When the power consumption cannot be maintained close to zero anymore, the reference is returned to a level close to baseline, and Alg. 2 is used for input following. Results are shown in Fig. 12. Different populations can take different time

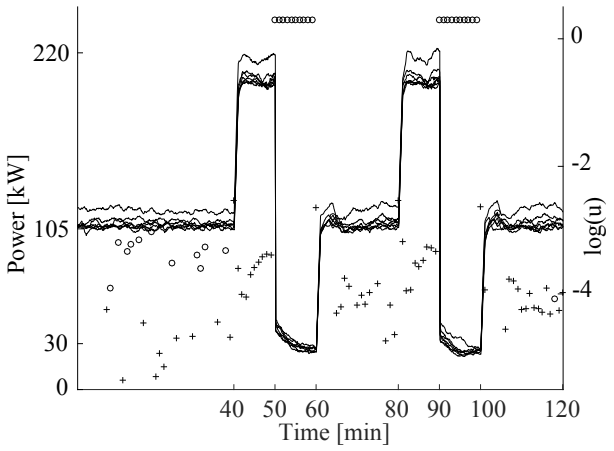

(a) Control of TCLs without minimum on/off timers

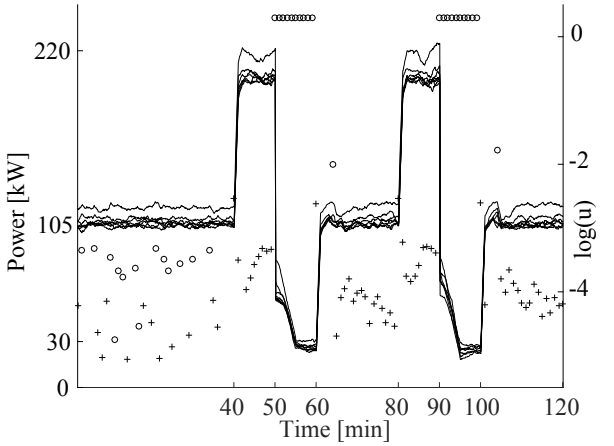

(b) Control of TCLs with minimum on/off timers

Fig. 10. Switching-Rate actuation, Alg. 2, Reference I. The plots shows overlapped results from the one homogeneous and the six heterogeneous populations. The baseline levels of each population are slightly different. The biggest errors occurs for the largest tested dispersion of the parameters (the uniform distribution with a standard parameter deviation of 30%). The input rates, corresponding to one of the simulations only, are plotted logarithmically. Marker "o" is used u_0 values, and marker "+" is used for u_1 values.

finish the storage control phase (the time increasing with heterogeneity), and the duration of the discharge period (the zero consumption period) is also different between populations, and decreasing with heterogeneity.

Both control techniques can handle some amount of heterogeneity, with the biggest errors occurring for the largest tested dispersion of the parameters, i.e. the uniform distribution with a standard parameter deviation of 30%.

Furthermore, the above algorithms have not been using individual unit measurements and have not updated the internal model. As such the internal model is running in open loop, and the errors are increasing in time, especially for heterogeneous populations. Updating the internal models periodically using the measurements and estimation techniques will improve the performance of the control algorithms.

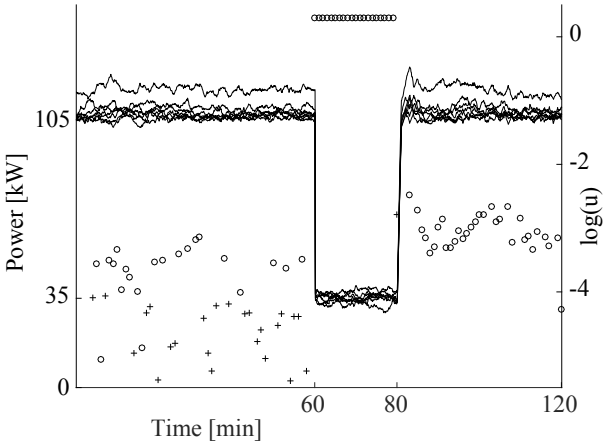

(a) Control of TCLs without minimum on/off timers

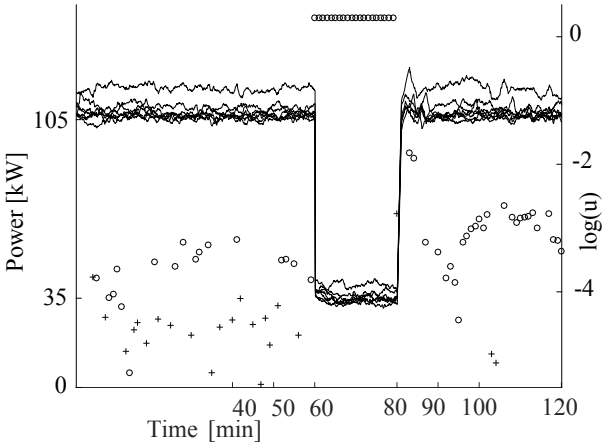

(b) Control of TCLs with minimum on/off timers

Fig. 11. Switching-Rate, Control Alg. 2, Reference II, same format as Fig. 10.

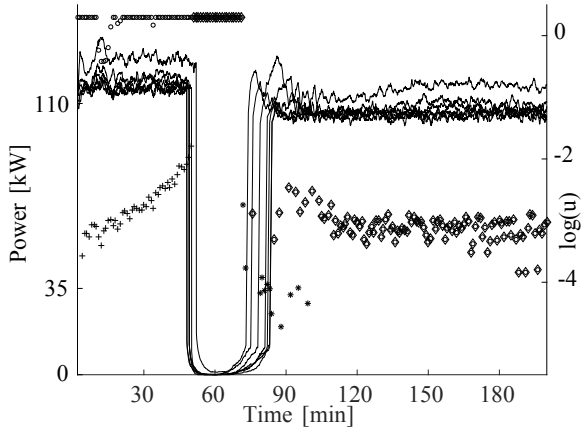

(a) Control of TCLs without minimum on/off timers

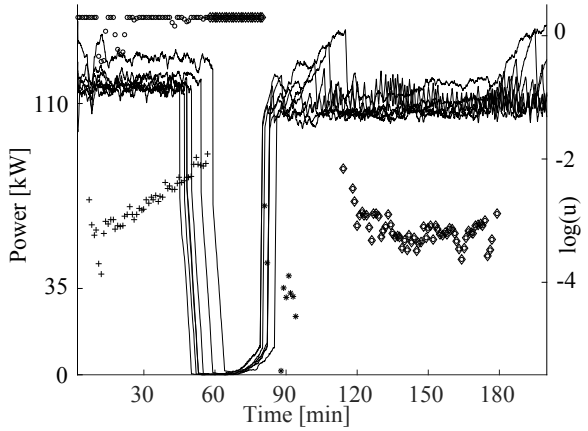

(b) Control of TCLs with minimum on/off timers

Fig. 12. Switching Rate, Control Alg. 3. The Storage phase takes place up until approximately minute 50, the Discharge or step-down phase takes place between minutes 50 and 90 approximately, and the Recover phase consisting of the input tracking control Alg. 2 with a baseline reference takes place after minute 90. The input rates, corresponding to one of the simulations only, are shown in a logarithmic scale. Marker o is used u_{0b_2}, marker $\diamond$ is used for u_{0b_3}, marker $\times$ is used for u_{1b_1}, and marker $+$ is used for u_{1b_2}.

V. Conclusion and future work

This work has proposed a new, practical actuation strategy for enabling large scale demand response of thermostatic loads. The Switching-Rate actuation has been described, modeled and used to activate the power consumption flexibility of a population of thermostatic loads in a numerical scenario. It complements the range of flexibility options that can be proposed to a refrigerator user for participation in a demand response program, and the range of actions available to a system utility operator.

Additionally, several directions for future work open up as a result of the promising numerical scenario. First, it would be of interest to study the actuation in a demonstration setup, subject to the real thermal and population dynamics, and under realistic disturbances (e.g., including door-opening events). Secondly, we note that more advanced control issues remain open. For example, neither Alg. 2 nor Alg. 3 return the distribution state to equilibrium, and thus stopping the control broadcast returns the system to a free response with oscillatory output behavior before the equilibrium state is reached. The problem of a controlled return to the equilibrium state should be addressed by future work. Furthermore, it is clear that not all power references are tractable. The problem of describing tractable references for a TCL population depends not only on the population parameters, but also on the control algorithm, and has not been addressed. Thirdly, we point to problem of reducing the system dimensionality. In this work, the PDE dynamics have been brought to a finite dimensional, continuous-time form using FVM as numerical techniques. However, FVM do not generally preserve structural properties such as positivity of the dynamical system, while the special technique in [36] has the disadvantage of producing very large matrices not directly suitable for online algorithms. Model order reduction techniques for bilinear systems could be tested in future work. Finally, it would be of interest to preform quantitative comparisons on power reference tracking scenarios and analyze the performance of different fully responsive actuations.

Acknowledgment

This work has been supported by the Southern Denmark Growth Forum and the European Regional Development Fund under the project "Smart & Cool". The authors would like to extends thanks to Karl Damkjaer Hansen for his work setting up an instrumented refrigerator unit and practical insights. We would further like to thank the reviewers for their time and constructive contributions.

References

[1] "Global status report," Renewable Energy Policy Network for the 21st Century, 2014.

[2] European Wind Energy Association and others, *Large Scale Integration of Wind Energy in the European Power Supply: Analysis, Issues and Recommendations: a Report*. European Wind Energy Association, 2005.

[3] International Energy Agency, *The Power of Transformation Wind, Sun and the Economics of Flexible Power Systems*, 2014.

[4] I. Stadler, "Power grid balancing of energy systems with high renewable energy penetration by demand response," *Utilities Policy*, vol. 16, no. 2, pp. 90–98, 2008.

[5] J. Torriti, M. G. Hassan, and M. Leach, "Demand response experience in europe: Policies, programmes and implementation," *Energy*, vol. 35, no. 4, pp. 1575–1583, 2010.

[6] P. Palensky and D. Dietrich, "Demand side management: Demand response, intelligent energy systems, and smart loads," *Industrial Informatics, IEEE Transactions on*, vol. 7, no. 3, pp. 381–388, 2011.

[7] D. Hurley, P. Peterson, and M. Whited, "Demand response as a power system resource," 2013.

[8] D. S. Callaway and I. A. Hiskens, "Achieving controllability of electric loads," *Proceedings of the IEEE*, vol. 99, no. 1, pp. 184–199, 2011.

[9] A. C. Kizilkale and R. P. Malhame, "Collective target tracking mean field control for markovian jump-driven models of electric water heating loads," in *IFAC World Congress*, 2014.

[10] S. Ihara and F. C. Schweppe, "Physically based modeling of cold load pickup," *Power Apparatus and Systems, IEEE Transactions on*, no. 9, pp. 4142–4150, 1981.

[11] R. Malhame and C.-Y. Chong, "Electric load model synthesis by diffusion approximation of a high-order hybrid-state stochastic system," *Automatic Control, IEEE Transactions on*, vol. 30, no. 9, pp. 854–860, 1985.

[12] R. Mortensen and K. Haggerty, "A stochastic computer model for heating and cooling loads," *Power Systems, IEEE Transactions on*, vol. 3, no. 3, pp. 1213–1219, 1988.

[13] S. Esmaeil Zadeh Soudjani and A. Abate, "Aggregation and control of populations of thermostatically controlled loads by formal abstractions," *Control Systems Technology, IEEE Transactions on*, vol. PP, no. 99, pp. 1–1, 2015.

[14] D. S. Callaway, "Tapping the energy storage potential in electric loads to deliver load following and regulation, with application to wind energy," *Energy Conversion and Management*, vol. 50, no. 5, pp. 1389–1400, 2009.

[15] S. Bashash and H. K. Fathy, "Modeling and control of aggregate air conditioning loads for robust renewable power management," *Control Systems Technology, IEEE Transactions on*, vol. 21, no. 4, pp. 1318–1327, 2013.

[16] C. Perfumo, E. Kofman, J. H. Braslavsky, and J. K. Ward, "Load management: Model-based control of aggregate power for populations of thermostatically controlled loads," *Energy Conversion and Management*, vol. 55, pp. 36–48, 2012.

[17] J. Mathieu, S. Koch, and D. Callaway, "State estimation and control of electric loads to manage real-time energy imbalance," *Power Systems, IEEE Transactions on*, vol. 28, no. 1, pp. 430–440, Feb 2013.

[18] W. Zhang, J. Lian, C.-Y. Chang, and K. Kalsi, "Aggregated modeling and control of air conditioning loads for demand response," *IEEE Transactions on Power Systems*, vol. 28, no. 4, pp. 4655 – 4664, 2013.

[19] L. C. Totu, J. Leth, and R. Wisniewski, "Control for large scale demand response of thermostatic loads," in *American Control Conference (ACC)*. IEEE, 2013, pp. 5023–5028.

[20] L. C. Totu and R. Wisniewski, "Demand response of thermostatic loads by optimized switching-fraction broadcast," in *IFAC World Congress*, 2014.

[21] N. A. Sinitsyn, S. Kundu, and S. Backhaus, "Safe protocols for generating power pulses with heterogeneous populations of thermostatically controlled loads," *Energy Conversion and Management*, vol. 67, pp. 297–308, 2013.

[22] J. Bendtsen and S. Sridharan, "Efficient desynchronization of thermostatically controlled loads," *11th IFAC International Workshop on Adaptation and Learning in Control and Signal Processing*, 2013.

[23] M. Stadler, W. Krause, M. Sonnenschein, and U. Vogel, "Modelling and evaluation of control schemes for enhancing load shift of electricity demand for cooling devices," *Environmental Modelling & Software*, vol. 24, no. 2, pp. 285–295, 2009.

[24] L. C. Totu, R. Wisniewski, and J.-J. Leth, "Modeling populations of thermostatic loads with switching rate actuation," in *4th Hybrid Autonomous Systems (HAS) Workshop*, 2014.

[25] C.-Y. Chang, W. Zhang, J. Lian, and K. Kalsi, "Modeling and control of aggregated air conditioning loads under realistic conditions," in *Innovative Smart Grid Technologies (ISGT), 2013 IEEE PES*. IEEE, 2013, pp. 1–6.

[26] B. N. Borges, C. J. Hermes, J. M. Gonçalves, and C. Melo, "Transient simulation of household refrigerators: a semi-empirical quasi-steady approach," *Applied Energy*, vol. 88, no. 3, pp. 748–754, 2011.

[27] M. L. Bujorianu and J. Lygeros, "General stochastic hybrid systems: Modelling and optimal control," in *Decision and Control, 2004. CDC. 43rd IEEE Conference on*, vol. 2. IEEE, 2004, pp. 1872–1877.

[28] ——, "Toward a general theory of stochastic hybrid systems," in *Stochastic Hybrid Systems*. Springer, 2006, pp. 3–30.

[29] L. Totu, "Large scale demand response of thermostatic loads," Ph.D. dissertation, 2015.

[30] E. B. Dynkin, *Markov processes*. Springer, 1965.

[31] C. W. Gardiner, *Handbook of stochastic methods: for Physics, Chemistry and the Natural Sciences*. Springer Berlin, 1985.

[32] J. H. Ferziger and M. Perić, *Computational methods for fluid dynamics*. Springer Berlin, 2002, vol. 3.

[33] E. F. Toro, *Riemann solvers and numerical methods for fluid dynamics*. Springer, 1999, vol. 16.

[34] A. Ghaffari, S. Moura, and M. Krstic, "Analytic modeling and integral control of heterogeneous thermostatically controlled load populations," in *Dynamic Systems and Control Conference, ASME Proceedings*, 2014.

[35] L. Farina and S. Rinaldi, *Positive linear systems: theory and applications*. John Wiley & Sons, 2011, vol. 50.

[36] J. C. Latorre, P. Metzner, C. Hartmann, and C. Schütte, "A structure-preserving numerical discretization of reversible diffusions," *Commun. Math. Sci*, vol. 9, no. 4, pp. 1051–1072, 2011.

[37] P. M. Pardalos and V. A. Yatsenko, *Optimization and Control of Bilinear Systems: Theory, Algorithms, and Applications*. Springer Science & Business Media, 2010, vol. 11.

[38] R. R. Mohler and W. Kolodziej, "An overview of bilinear system theory and applications," *IEEE Transactions on Systems, Man and Cybernetics*, vol. 10, no. 10, pp. 683–688, 1980.

[39] H. K. Khalil, *Nonlinear systems*. Prentice Hall Upper Saddle River, 2002, vol. 3.

[40] F. Gembicki, "Vector optimization for control with performance and parameter sensitivity indices," Ph.D. dissertation, Ph.D. Thesis, Case Western Reserve Univ., Cleveland, Ohio, 1974.